



Boundary slip moderated by interfacial hydrogen bond dynamics

JinChuan Li¹ · KeLi Zhang¹ · JingCun Fan¹ · HengAn Wu¹ · FengChao Wang¹

Received: 19 July 2023 / Accepted: 11 October 2023 / Published online: 2 November 2023
© The Author(s), under exclusive licence to Springer-Verlag GmbH Germany, part of Springer Nature 2023

Abstract

Understanding the slip behaviors on the graphene surfaces is crucial in the field of nanofluidics and nanofluids. The reported values of the slip length in the literature from both experimental measurements and simulations are quite scattered. The presence of low concentrations of functional groups may have a greater impact on the flow behavior than expected. Using non-equilibrium molecular dynamics simulations, we specifically investigated the influence of hydroxyl-functionalized graphene surfaces on the boundary slip, particularly the effects related to hydrogen bond dynamics. We observed that hydroxyl groups significantly hindered the sliding motion of neighboring water molecules. Hydrogen bonds can be found between hydroxyl groups and water molecules. During the flow process, these hydrogen bonds continuously form and break, resulting in the energy dissipation. We analyzed the energy balance under different driving forces and proposed a theoretical model to describe the slip length which also considers the influence of hydrogen bond dynamics. The effects of the driving force and the surface functional group concentration were also studied.

Keywords Boundary slip · Hydrogen bond · Nanoflow · MD simulations

1 Introduction

The research on the fluid flow in nanochannels is of great significance both practically and fundamentally (Kannam et al. 2013). The development of nanofluidics offers inspiring solutions in various applications, including chromatography, drug delivery, chemical separations, water desalination, and sustainable energies (Eijkel and van den Berg 2005; Schoch et al. 2008; Zhang et al. 2020). Despite significant efforts over the years, the underlying mechanisms governing fluid behavior at the nanoscale remain elusive (Figoli et al. 2017). The behavior of fluids at the nanoscale often departs from the traditional framework of continuum theory, which describes fluid behavior on macroscopic scales (Bocquet and Charlaix 2010; Kavokine et al. 2021).

In recent years, numerous experimental measurements and simulations have suggested that ultrafast water

transport takes place inside carbon nanotubes (CNTs) and nanochannels constructed using graphene sheets (Whitby and Quirke 2007; Falk et al. 2010; Ye et al. 2011; Kannam et al. 2013; Guo et al. 2015; Secchi et al. 2016). In the microfabricated membranes composed of aligned CNTs with diameters less than 2 nm, the water flow was measured to exceed the predicted values from Poiseuille law by more than 3–5 orders of magnitude (Hummer et al. 2001). Experiments reported that the velocity of water transport through graphene nanoslits with a height of about 1 nm can reach up to 1 m/s (Radha et al. 2016). One important reason for these fast water flow is the large slip length at the water/graphene interface. The slip length, which characterizes the degree of slip, plays a crucial role in theoretical calculations. Many experimental and theoretical studies have studied the slip length of water on graphene surfaces, but the reported results still exhibit significant discrepancies, which span the range of 1–80 nm (Kannam et al. 2013). Based on the experimental results, the slip length of water flow in CNTs shows strongly radius dependent. It can be as large as 300 nm for CNTs with a radius of about 15 nm. However, almost no slip occurred for the water flow inside boron nitride (BN) nanotubes (Secchi et al. 2016). The differences in friction forces between these two surfaces were insufficient to explain

✉ HengAn Wu
wuha@ustc.edu.cn

✉ FengChao Wang
wangfc@ustc.edu.cn

¹ CAS Key Laboratory of Mechanical Behavior and Design of Materials, Department of Modern Mechanics, University of Science and Technology of China, Hefei 230027, China

the disparity in slip lengths (Tocci et al. 2014). Therefore, the significant differences in slip lengths should originate from more subtle atomic-scale details at the solid–liquid interface, including defects or electronic structures of the wall material (Secchi et al. 2016). In molecular dynamics (MD) simulations, the channel walls are usually modeled as atomically smooth graphitic surfaces (Joly et al. 2016; Michaelides 2016; Grosjean et al. 2016). Most simulation models did not fully consider the influence of surface defects, functional groups, and water dissociation on the solid surface (Majumder et al. 2011; Vijayaraghavan and Wong 2014). In actual experiments, low concentrations of defects and residual functional groups may have a greater impact on the flow behavior than expected.

Density functional theory (DFT) calculations were performed to investigate the adsorption of hydroxyl functional groups in water environments on monolayer graphene and hexagonal BN surfaces. The results show that the hexagonal BN surface is more prone to the adsorption of hydroxyl functional groups compared to the graphene surface, due to the difference in electronic structure of the surface materials (Grosjean et al. 2016). Water friction on several defective surfaces was computed using ab initio molecular dynamics (AIMD) simulations. It was observed that at certain specific defects, water molecules dissociated into ion groups and adsorbed onto the surface. In addition, at these defect sites, surface groups formed additional hydrogen bonds (H-bonds) with other water molecules, significantly enhancing the solid–liquid frictional forces. The enhanced friction could be as high as eight times of that on a smooth surface (Joly et al. 2016). Other MD simulations revealed that even a very low concentration of hydroxyl functional groups (~5%) on the graphene surface reduced the slip length of water flow by 97%, decreasing it from 48 to 1.26 nm (Wei et al. 2014a). The influence of hydroxyl-functionalized graphene surfaces on the flow of confined two-dimensional water in a slit channel was investigated using MD simulations (Fang et al. 2018). Although the water flow was not completely blocked at the edge of the hydroxyl functional groups, they still significantly impeded the flow. The resistance generated by a single, isolated hydroxyl functional group was equivalent to an area of ~90 nm² of pristine graphene surface (Fang et al. 2018).

It is important to fully understand how the presence of functional groups on the graphene sheet can significantly reduce the water flow. In this study, we intend to go deeper on this problem. Using non-equilibrium MD simulations, the dynamic behavior of H-bonds at the interface and the influence on boundary slip behavior were investigated. The H-bond breaking rate was calculated under different driving forces on the water flow. Based on the energy analysis, a theoretical model was proposed to explain how the interfacial H-bond dynamics moderates the boundary slip.

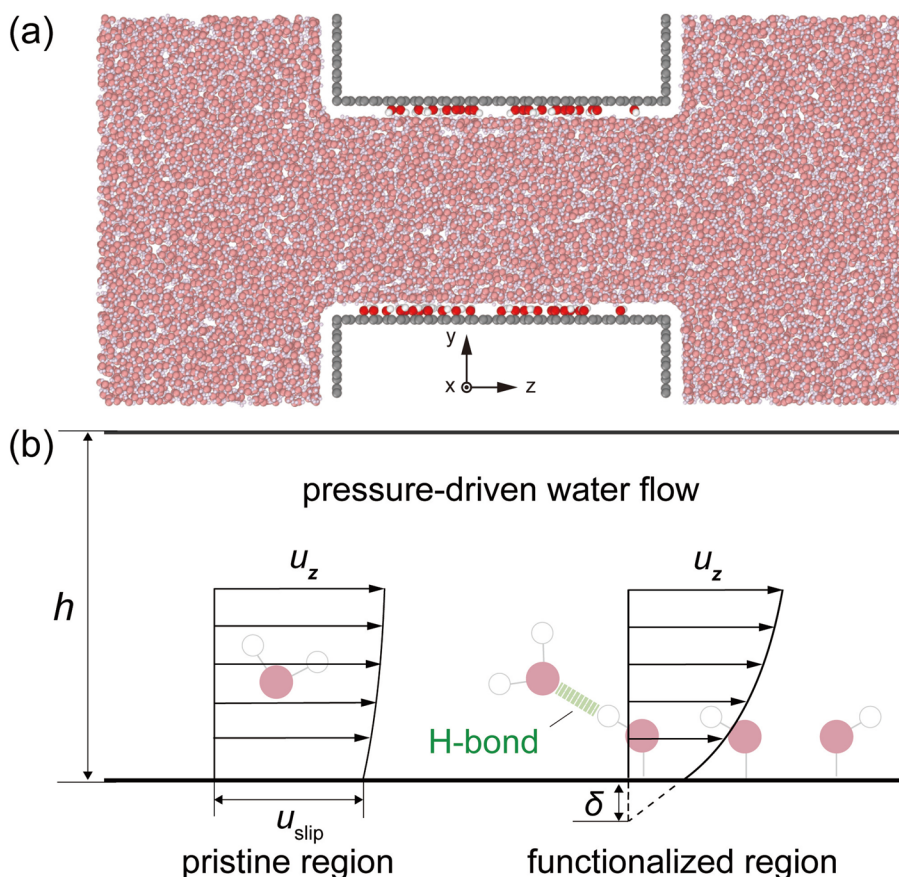
2 Methods

To investigate the influence of H-bond dynamics on the boundary slip behavior of water flow, we created a nano-channel using two parallel graphene sheets. The channel connects two water reservoirs each containing 5000 molecules, as shown in Fig. 1a. The graphene sheets featuring hydroxyl groups have the lateral xy dimension of 5.11×5.11 nm². The channel height is defined as the center-to-center distance between the carbon atoms of two graphene walls, which is 3.4 nm. Hydroxyl-functionalized graphene channels were constructed with different surface functional group concentrations, denoted as c . $c = n_{\text{OH}}/n_{\text{C}}$, where n_{OH} and n_{C} represent the number of hydroxyl groups and carbon atoms on the wall, respectively. The value of c ranges from 0 to 5%. It was reported that functional groups tend to form aggregation on graphene surfaces (Erickson et al. 2010; Yan and Chou 2010; Mouhat et al. 2020; Guo et al. 2022). Therefore, in our simulation model, the oxidized carbon atoms were not fully randomly distributed. We arranged the functional groups to form cluster distributions on the channel walls. On the upper and lower walls of the channel, we selected two circular regions where the hydroxyl groups were distributed. Thus, there are two types of regions: the functionalized regions with hydroxyl groups and the pristine regions without hydroxyl groups.

The hydroxyl group atoms (including hydrogen and oxygen atoms) were allowed to move, providing flexibility of the surface functional groups. The bond stretching and angle bending of the hydroxyl groups were taken into account explicitly. All carbon atoms were fixed during MD simulations. The force field employed in this work consisted the Lennard–Jones (LJ) potential and the electrostatic term with Coulomb's law. A cutoff of 1 nm was used. The long-range Coulombic interactions were calculated used the particle–particle particle–mesh (PPPM) method.

There are a large number of computer simulation studies that evaluated several water models, including SPC, SPC/E (rigid extended simple point charge), TIP4P, TIP5P, TIP4P/2005, TIP4P-BG, etc. (Mark and Nilsson 2001; Abascal and Vega 2005; Wu et al. 2006; Ho and Striolo 2014; Ye et al. 2021). Indeed, careful analysis of many thermodynamical, dynamical, and structural properties shows that SPC/E model performs well: the water shear viscosity, self-diffusion constant, static dielectric constant, etc. (Smith and van Gunsteren 1993; Wu et al. 2006; González and Abascal 2010). Therefore, the SPC/E model has also been extensively used in a substantial body of research on the interactions between water and graphene (Argyris et al. 2008; Sala et al. 2012; Taherian et al. 2013; Kalluri et al. 2013). Nowadays, based on machine learning and other methods, some water molecule models

Fig. 1 a Snapshot of the MD model for studying water flow in a graphene channel with an interlayer distance equal to 3.4 nm. On each end of the channel, a water reservoir is connected, and both channel sheets are decorated with hydroxyl groups. The red, white, and gray spheres denote water oxygen, hydroxyl oxygen, hydrogen, and carbon atoms, respectively. **b** Schematic representation of water flow through the pristine and functionalized region on channel walls, including H-bonds between hydroxyl groups and water molecules. The horizontal black lines denote the graphene sheet, while oxygen and hydrogen atoms are shown as red and white spheres, respectively



with excellent performance have been developed, such as TIP4P-BG and TIP4P-BGT (Ye et al. 2021). In our study, the SPC/E model (Berendsen et al. 1987) was used for the water molecules. The LJ parameters governing the interaction between graphene and water are as follows: $\sigma_{CO} = 3.436 \text{ \AA}$, $\epsilon_{CO} = 0.0850 \text{ kcal/mole}$, $\sigma_{CH} = 2.690 \text{ \AA}$, and $\epsilon_{CH} = 0.0383 \text{ kcal/mole}$ (Wu and Aluru 2013). The parameters for the LJ interactions, bond and angle interactions of hydroxyl groups and graphene were determined using the optimized potential for liquid simulations-all atom (OPLS-AA) force field (Jorgensen et al. 1996), which is commonly used to simulate graphene with surface functional groups (Wei et al. 2014b; Chen et al. 2017). Periodic boundary conditions were applied in all the three directions.

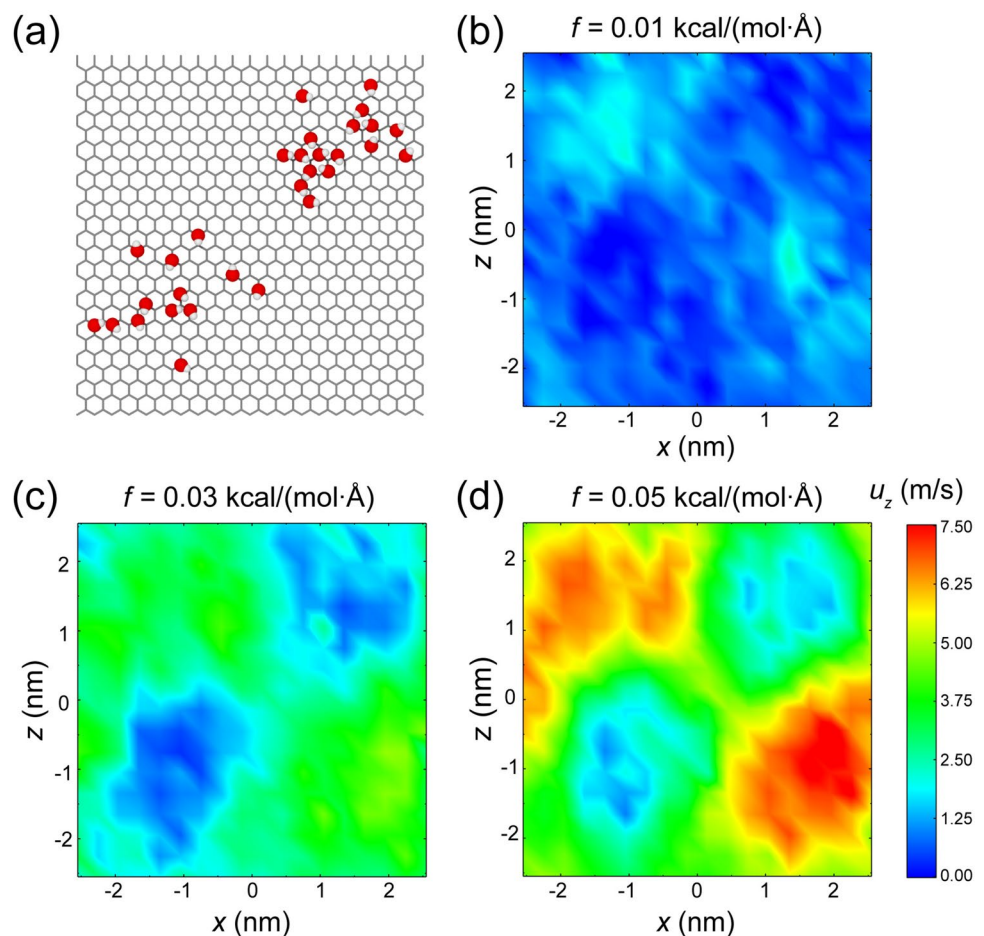
MD simulations were performed using the large-scale atomic/molecular massively parallel simulator (LAMMPS) package (Plimpton 1995). A time step of 1.0 fs was used for the velocity-Verlet integrator, with the SHAKE algorithm applied for the water to reduce high-frequency vibrations that need shorter time steps. The temperature and pressure were controlled by the Nosé–Hoover thermostat and barostat, respectively. To calculate the temperature, the spatially averaged center-of-mass velocity was subtracted out in the calculation on the kinetic energy. Initially, simulations

were carried out in constant pressure and temperature (NPT) ensemble. All water molecules were equilibrated for 200 ps at a temperature of 298 K and pressure of 1 atm to reach equilibrium. The graphene channels were initially empty and then filled with water molecules. The length of the simulated box along the z -axis changed accordingly. Then non-equilibrium MD simulations were performed in the canonical (NVT) ensemble to investigate the fluid flow. To drive the flow, a constant force was applied to water molecules in a minute rectangular region from $z = -6.23$ to -6.13 nm at the end of the simulation box.

3 Results and discussion

We first examined how the presence of hydroxyl groups affects the motion of water molecules at the interface. In our MD simulations, the velocities of on graphene surfaces with various c and under different driving forces were calculated. Here the channel with $c = 3\%$ was taken as an example. The distribution of hydroxyl groups on the upper surface is shown in Fig. 2a. The upper and lower walls of the channel have the same c and similar distributions of hydroxyl groups. To investigate the effect of various driving forces, we applied three different magnitudes of driving forces: $f = 0.01, 0.03,$

Fig. 2 **a** Structure of hydroxyl-functionalized graphene sheet with functional group concentrations $c = 3\%$. Red and white spheres on gray graphene represent hydrogen atoms and oxygen atoms in hydroxyl groups, respectively. **b–d** The distribution of z -direction water boundary slip velocity u_z in the xz -plane with driving force applied along the z -direction: $f = 0.01, 0.03, 0.05$ kcal/(mole Å), respectively. Only the water molecules in the interfacial layer were considered



0.05 kcal/(mol Å). After MD simulations of 20 ns, the water flow reached a steady state under the applied driving forces. A region located approximately 0.2 nm away from the channel walls and with a width of approximately 0.3 nm was defined as the interface layer. The water molecules within this interfacial layer were identified and their velocities were calculated. The averaged velocity in this interfacial layer can also be regarded as the boundary slip velocity. The velocity contours of this water layer in the two-dimensional xz -plane were plotted for different driving forces in Fig. 2b–d.

Generally, the interfacial water flow exhibits larger velocity in the pristine regions, compared with that in the functionalized regions. At a driving force of $f = 0.01$ kcal/(mole Å), the velocity in the pristine regions is not high, which is about 1.5 m/s. In contrast, we cannot find notable slip velocity in the functionalized regions or nearby. That is to say, most water molecules in the functionalized regions have a velocity close to zero, as shown in Fig. 2b. If we averaged the velocity over the entire interfacial water layer, the slip velocity is not particularly significant. We can say there is not interfacial slip at this low driving force. As the driving force slightly increases to $f = 0.03$ kcal/(mole Å), the velocity difference between the pristine regions and the

functionalized regions becomes evident, as shown in Fig. 2c. The presence of hydroxyl groups clearly hinders the velocity of water molecules in the functionalized regions. Under a higher driving force of $f = 0.05$ kcal/(mole Å), a significant slip velocity exhibits even in the functionalized regions, reaching 1–2 m/s, as shown in Fig. 2d. At this point, we may say that the slip occurs in the entire interfacial water layer. These results again confirmed that the presence of hydroxyl groups on the channel walls hinders the motion of water molecules. H-bonds can be formed between the interfacial water molecules and the hydroxyl groups. The movement of water molecules in the interfacial layer must be accompanied by breaking of the H-bonds. Thus, the presence of hydroxyl groups creates significant resistance to the interfacial flow field and has a significant impact on boundary slip velocity. At lower driving forces, it is difficult for water flow to undergo the slip in the regions adjacent to the hydroxyl groups. As the driving force increases, the boundary slip is hindered by H-bonds, not only in the functionalized regions but also in the pristine regions. Meanwhile, the differences in the velocity between functionalized and pristine regions become more pronounced. The results above indicate that the occurrence of slip is more complicated than

we previously thought. There might be a transition process from no slip to slip at the boundary if the channel surfaces are not atomically smooth. The hydroxyl groups lead to a non-uniform distribution of slip velocity within the interfacial water layer, as shown in Fig. 2b–d. Because the driving force is gradually increasing, the entire interfacial water layer does not exhibit slip initially. Then the water flow in the pristine regions starts to slip. Next, the slip can be found in the functionalized regions. Finally, the entire interfacial water layer starts to slip.

The aforementioned interfacial water layer can be clearly seen in the density profiles of water along the direction perpendicular to the channel wall, as shown in Fig. 3a. There is a distinct density peak close to the channel wall. The density profiles exhibit profound decaying oscillation adjacent to two walls. In the center part of channels ($-0.5 \text{ nm} \leq y \leq 0.5 \text{ nm}$), the density is equal to the bulk density of water. We can find from Fig. 3a that the density profiles are almost the same under different driving forces. We calculated the velocity profiles along the direction perpendicular to the channel

wall, as shown in Fig. 3b. The flow velocity in an intermediate region of the channel ($-1.7 \text{ nm} \leq y \leq 1.7 \text{ nm}$, $-1.5 \text{ nm} \leq z \leq 1.5 \text{ nm}$) under different driving force was averaged. It can be observed that the flow velocity at the boundary is significantly influenced by the presence of hydroxyl groups. The characteristics of these velocity profiles can be described theoretically by the Poiseuille flow with slip boundary conditions,

$$u(y) = \frac{P}{2\eta L} \left(\frac{h^2}{4} - y^2 \right) + u_{\text{slip}}, \tag{1}$$

where η is the shear viscosity, P/L is the pressure gradient along the flow direction, u_{slip} is the slip velocity at the fluid–wall interface, and h is the effective width of the channel along the y -axis. According to the definition of the Navier’s slip boundary condition (Navier 1823; Eslami and Müller-Plathe 2010), the slip velocity u_{slip} at the wall is proportional to the normal derivative of the velocity. The slip length δ of the boundary water layer:

$$\delta = \frac{u(y)}{du/dy} \Big|_{y=\pm h/2} = \frac{2\eta L}{\Delta Ph} u_{\text{slip}}. \tag{2}$$

The overall average slip velocity of the boundary water layer increases from ~ 0 to ~ 3 m/s, which corresponds to the onset of slip behavior. The slip velocity calculated from the interfacial water layer increases with the increasing driving force. Examining the velocity curve in Fig. 3a, it is noticed that the slip velocity at the boundary deviates from the fitted parabolic profile. This result is expected because a layered and ordered structure of water molecules occurs at the interface.

From Eq. (1), we can see that the pressure gradient P/L is important in determining the velocity inside the channel. Although the pressure gradient cannot be estimated directly from the driving force, we can use two other methods to calculate the pressure gradient inside the channel. First, the pressure distribution along the flow direction in the channel can be obtained by fitting the velocity parabola in Fig. 3a using Eq. (1). P/L can be obtained from the coefficient of the quadratic term of the quadratic curve. In addition, the pressure distribution along the flow direction can also be calculated using the Irving–Kirkwood (IK) formula (Irving and Kirkwood 2004; Yang et al. 2012), as shown in the inset of Fig. 4. The pressure gradient can be obtained by calculating the slope of the pressure distribution with respect to the distance along the channel. These results under different driving forces are summarized in Fig. 4. The pressure gradient obtained by the two methods show quite good agreement.

The pressure gradient obtained in Fig. 4 provides the driving force for the water flow. At the channel wall surfaces, there are interactions between the hydroxyl groups and water

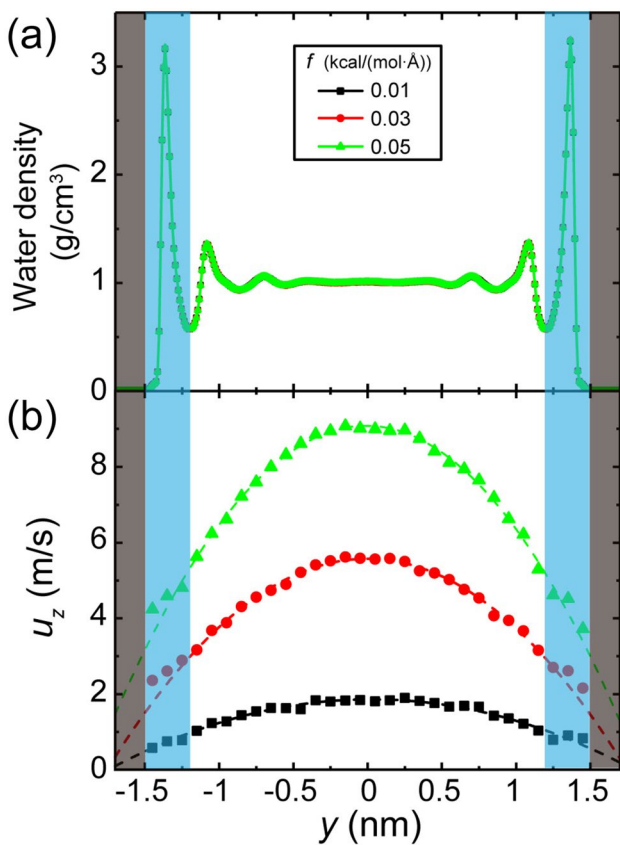


Fig. 3 **a** Density profiles and **b** velocity profiles of water flow within the channel are shown. Water flows between the sheets with a functional group concentration of $c = 3\%$ and under different driving forces. The range of driving force f is from 0.01 to 0.05 kcal/(mol Å). In **a**, **b**, the position of the interface layer is represented by the blue region, while the channel walls are represented by the black region

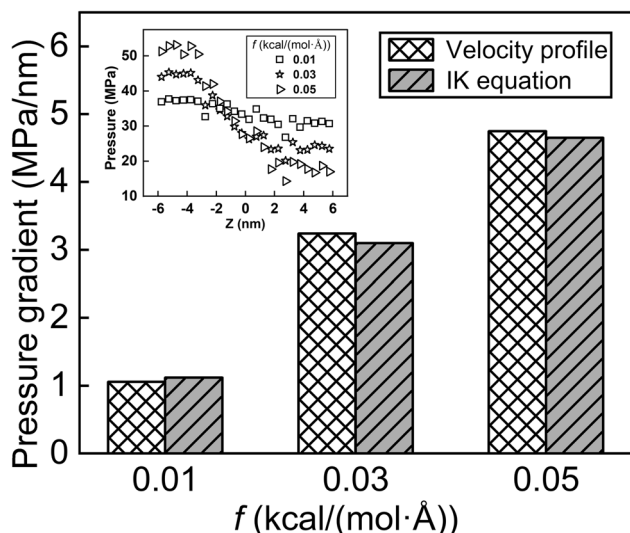
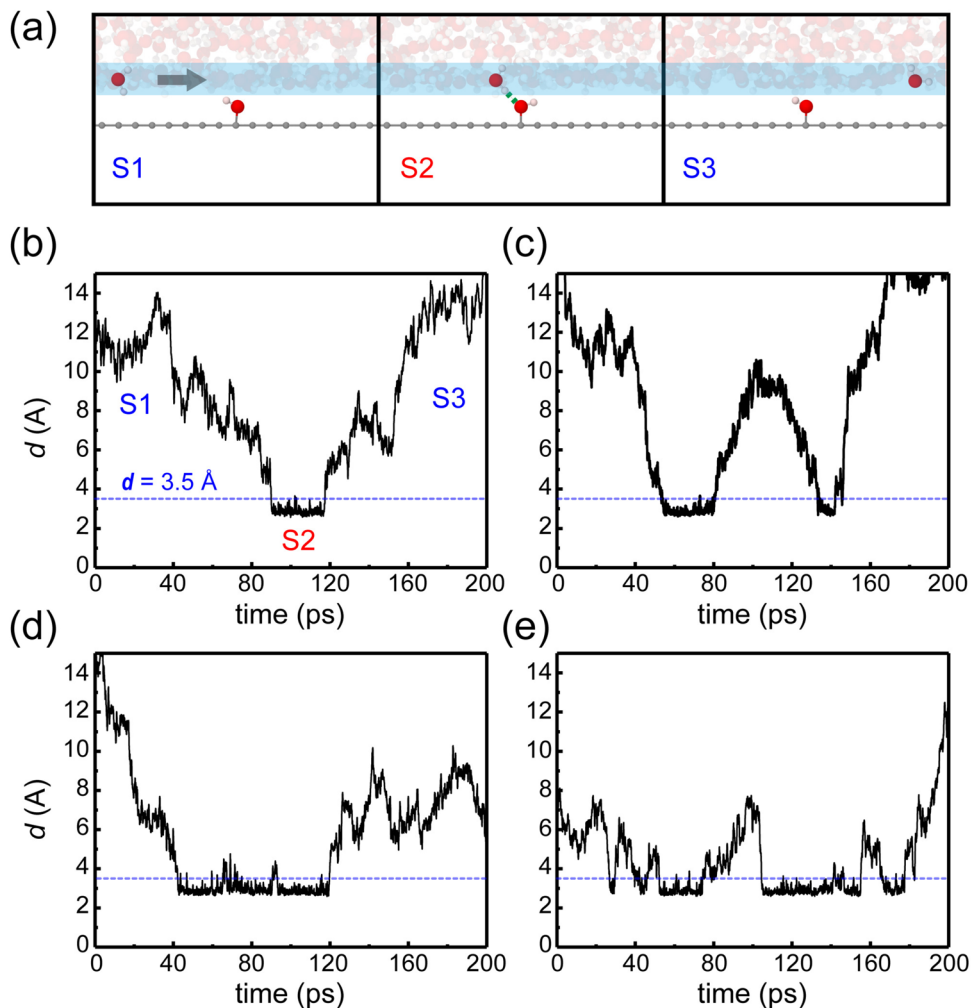


Fig. 4 The comparison of calculated pressure gradient in the channel using two different methods: fitting the velocity profiles with Eq. (1), and calculating the pressure distribution using the IK equation. The inset illustrates the pressure distribution in the channel for different driving forces obtained using the IK formula

Fig. 5 a Three typical states in the dynamic behavior of a H-bond: initial state (S1), formation (S2), and breaking (S3). The light blue region represents the water layer closest to the wall, and the black arrows indicate the direction of water molecule motion. **b–e** The variation of the oxygen–oxygen distance d between water molecules and the hydroxyl groups over time t . Four examples are provided. The blue dashed line represents the criterion of H-bond formation. When $d < 3.5 \text{ \AA}$, it indicates the formation of H-bonds between water molecules and hydroxyl groups



molecules in the interfacial water layer. The non-uniform distribution of slip velocity along the wall surface shown in Fig. 2 indicates that the presence of hydroxyl groups hinders the boundary slip. We believe that H-bonds formed between the hydroxyl groups and water molecules is the main cause of this hindrance. The H-bonds mentioned here and later just refer to the H-bonds between water molecules and hydroxyl groups, not that among water molecules.

To understand the mechanism of how the H-bonds hinder the slip behavior, we investigated the dynamic processes of H-bond formation and breaking. As shown in Fig. 5a, we focus on one water molecule and a hydroxyl group. Functional groups only form H-bonds with water molecules in the layer closest to the surface. Due to molecular thermal motion, water molecules near the functional groups exhibit diverse movement directions. Water molecules moving in various directions can impact H-bonding; for example, the diffusion of water molecules in the direction perpendicular to the surface is slow and anisotropic. However, in our study, the influence of the driving force on H-bonds is mainly manifested in the fact that the driving force induces

water molecules to flow along the z -direction, leading to the formation of H-bonds as water molecules pass the functional groups. Subsequently, the driving force causes them to move away from the functional groups in the z -direction, resulting in bond breaking.

In our research, there are three typical states in the dynamic behavior of a H-bond. (i) Initial state: there is no H-bond between this water molecule and the hydroxyl group. The hydroxyl group might connect with another water molecule by a H-bond. This state is referred to as S1. (ii) H-bond formation: this water molecule and the hydroxyl group are connected by the H-bond, which is called S2. (iii) H-bond breaking (S3): this water molecule separated with the hydroxyl group. When a H-bond forms, the oxygen and hydrogen atoms in hydroxyl groups can act as either donors or acceptors. Each hydroxyl group typically forms 1–3 H-bonds with adjacent water molecules.

To determine the formation of H-bonds, the geometric method proposed by Luzar and Chandler (1996a, b) was employed in our analysis. The distance d between the oxygen atom of a water molecule and the oxygen atom of a hydroxyl group is less than 3.5 \AA , it is considered that a H-bond has formed between them. Before calculating the number of H-bonds at each time step, we performed an average analysis of the distances d between oxygen atoms to minimize the random effects caused by molecular thermal fluctuations. After observing the vibrational behavior of water molecules, we averaged the distance between oxygen atoms d , over a period of 100 fs:

$$d_{\text{new}}(t) = \sum_0^n d_i/n. \tag{3}$$

The time evolution of the statistically averaged distance d was performed for each hydroxyl group. Some of the typical examples are provided in Fig. 5b–e. When the water molecules are not forming H-bonds with the hydroxyl groups, the value of d is greater than 3.5 \AA . This state is referred to as S1, as illustrated in Fig. 5b. When the water molecules approach the hydroxyl groups closely enough, H-bonds start

to form, and the value of d stabilizes below 3.5 \AA for a certain period of time. The curve of d as a function of time exhibits a clear plateau, indicating the stable formation of H-bonds, which corresponds to the state S2. The lifetime of the H-bonds, represented by the duration of the plateau of d , is approximately between 10 and 100 ps. Subsequently, the water molecules may escape from the hydroxyl groups. Then d is larger than 3.5 \AA , representing the breaking of the H-bonds, referred to as state S3.

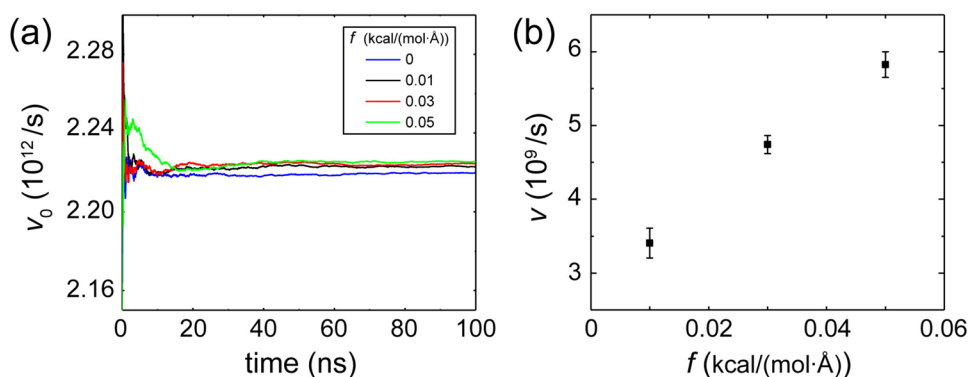
This method allowed us to conduct detailed analysis on the time evolution of the H-bond breaking rate ν_0 in the interfacial water layer under different driving forces. The results are summarized in Fig. 6a. The analysis on the H-bond dynamics was performed for a sufficiently long time (100 ns) to obtain stable values of ν_0 . Although the H-bond breaking rate ν_0 exhibits some fluctuations in the first few tens of nanoseconds, its value eventually stabilizes. We also found that the H-bond breaking rate ν_0 increases with the increasing driving force. Even in the absence of driving force, the formation and breaking of H-bonds occurs frequently due to molecular thermal motion, as shown in the case of $f = 0$ in Fig. 6a. Therefore, when we intend to discuss the breaking rate of H-bonds as the outcome of the driving force, the H-bond breaking rate ν_0 when $f = 0$ should be subtract. That is

$$\nu(f) = \nu_0(f) - \nu_0(0). \tag{4}$$

This difference in H-bond breaking rate, $\nu(f)$, represents the contribution from the driving force. We refer to this as the driving H-bond breaking rate. The results given in Fig. 6b manifest that the driving H-bond breaking rate shows a proportional increase with the driving force. This indicates that the driving force significantly accelerates the dynamic process of H-bond breaking in the interfacial water layer.

The breaking of H-bonds is accompanied by energy exchange. The energy dissipation of the water flow has significant impact on the slip behavior at the solid–liquid interface. Considering the entire system consisting of the

Fig. 6 **a** The time variation of the H-bond breaking rate ν_0 during MD simulations of 100 ns under different magnitudes of driving forces f . **b** The relationship between the driving H-bond breaking rate ν and the driving force f . After ν_0 has reached a stable value, the results of ν were averaged over a time duration of 10 ns



water flow and the channel walls in MD simulation, the input energy rate to the system comes from the work done by the external driving force per unit time, which leads to the flow behavior caused by the pressure gradient. Eventually, the flow velocity inside the channel reaches a steady state, and the flow field becomes stationary. From an energy perspective, the work done by the pressure gradient on the system is ultimately dissipated, resulting in the energy balance of the system. The energy dissipation rate of the system can be divided into three parts. (1) The energy dissipation rate due to viscous stress W_{vis} . (2) The energy dissipation rate because of the water friction in the pristine regions, W_{fr} . This can be understood by the friction between water and the pristine graphene surface. (3) The third part of the energy dissipation rate is caused by H-bond breaking in the functionalized regions, W_{Hb} . So, we have

$$W_{\text{p}} = W_{\text{diss}} = W_{\text{vis}} + W_{\text{Hb}} + W_{\text{fr}}. \quad (5)$$

According to Eq. (1), the work done by the driving force can be calculated as:

$$W_{\text{p}} = \int_{-h/2}^{h/2} Pwu(y)dy = \frac{wh^3P^2}{12\eta L} + whPu_{\text{slip}}. \quad (6)$$

We can also obtain the energy dissipation rate W_{vis} caused by the internal viscous stress of the water flow:

$$W_{\text{vis}} = \int_{y=-h/2}^{y=h/2} wL\eta \left[\frac{du(y)}{dy} \right]^2 dy = \frac{wh^3\Delta P^2}{12\eta L}. \quad (7)$$

Regarding the energy dissipation rate at the boundary, we first calculate the energy dissipation rate W_{fr} caused by the frictional between water and graphene. Thus,

$$W_{\text{fr}} = 2wL\lambda(u_{\text{slip}})^2, \quad (8)$$

in which the friction coefficient λ between water and graphene can be calculated using the Green–Kubo formula. On the other hand, the energy dissipated rate due to the breaking of H-bonds between water molecules and hydroxyl groups can be described as,

$$W_{\text{Hb}} = 2wLn_{\text{OH}}v(f)\Delta E_{\text{Hb}}, \quad (9)$$

where ΔE_{Hb} is the energy required for breaking a single H-bond, n_{OH} is the number of hydroxyl groups on each graphene wall, and the coefficient 2 means there are two channel walls. There is an alternative method to calculate W_{Hb} when the value of ΔE_{Hb} is not easy to obtain:

$$W_{\text{Hb}} = F_z u_{\text{slip}}, \quad (10)$$

in which F_z is the friction force between water molecules and all the hydroxyl groups and u_{slip} is the slip velocity at the boundary. We speculate that Eqs. (9) and (10) provide similar results. However, one may also regard that the H-bond structures between water molecules and hydroxyl groups are different from that among water molecules in the bulk water. The calculation on the energy required for the H-bond breaking between a water molecule and a hydroxyl group needs in-depth analysis.

Using Eqs. (5–10), we calculated the values of each energy dissipation rate in the system and their proportions in the total energy dissipation, as shown in Fig. 7. We can find that the contribution from the frictional dissipation between the water molecules and the pristine graphene wall is extremely low. The main components are the viscous dissipation and the H-bond breaking dissipation. The proportions of these two components are inversely related and compete with each other. At lower driving forces [$f=0.01$ kcal/(mole \AA)], the energy dissipation caused by H-bonds is the dominant component. At this moment, the H-bond breaking dissipation accounts for 66% of the total dissipation, which is the primary obstacle to the boundary slip. However, as the driving force increases, the proportion of H-bond dissipation decreases significantly, and the viscous dissipation becomes the dominant component.

If there are no hydroxyl groups, the energy dissipation at the channel wall just comes from the friction between water molecules and the graphene surface. Under this circumstance, the energy balance Eq. (5) becomes:

$$W_{\text{p}} = W_{\text{vis}} + W_{\text{fr}}. \quad (11)$$

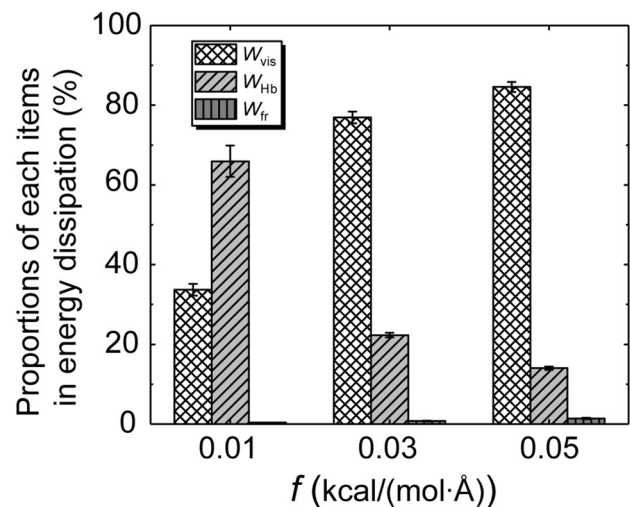


Fig. 7 The percentages of the three components in the total energy dissipation under different driving forces: the viscous dissipation W_{vis} , the H-bond breaking dissipation W_{Hb} , and the frictional dissipation W_{fr}

By substituting the specific expressions for each energy term, namely Eqs. (6–8) into Eq. (11), and using the relationship between slip length δ and slip velocity u_{slip} given by Eq. (2), we can obtain the slip length:

$$\delta = \frac{\eta}{\lambda}. \tag{12}$$

The expression for the slip length has been widely reported in the literature, which is used to calculate the slip length in MD simulations (Bocquet and Barrat 2007; Falk et al. 2010; Zhao 2012). Equation (12) indicates that the slip length δ is a ratio between a liquid property (viscosity η) and an interfacial property (friction coefficient λ). The friction coefficient λ can be obtained through the Green–Kubo equation in equilibrium molecular dynamics simulations (Falk et al. 2010; Bocquet and Barrat 2013; Li et al. 2021).

When the channel wall surface is functionalized by hydroxyl groups, the calculation of energy dissipation needs to include the dissipation due to H-bond breaking. In this case, the energy balance Eq. (5) includes three types of energy dissipation. By substituting the specific expressions for each energy component, we can obtain:

$$hPu_{\text{slip}} = L\lambda(u_{\text{slip}})^2 + Ln_{\text{OH}}\nu\Delta E_{\text{HB}}. \tag{13}$$

In the range of flow velocities considered in this study, we can approximately assume that there is a linear relationship between the slip velocity u_{slip} and the H-bond breaking rate ν . A characteristic length d_{HB} can be introduced:

$$d_{\text{HB}} = \frac{u_{\text{slip}}}{\nu}. \tag{14}$$

According to the linear fitting analysis of the MD simulation results, we found that the value of d_{HB} is approximately 4.7 Å. Then by substituting the definition of slip length δ from Eq. (12) into Eq. (13), we can derive the expression for slip length δ that incorporates the influence of H-bond breaking,

$$\delta = \frac{\eta}{\lambda} \left(1 - \frac{2n_{\text{OH}}\Delta E_{\text{HB}}}{d_{\text{HB}}hP/L} \right). \tag{15}$$

From Eq. (15), it seems that when $n_{\text{OH}} = 0$, it reduces to Eq. (13). We can also learn that if the pressure gradient induced by the driving force is extremely small at the beginning of the flow, the slip length calculated from Eq. (15) gives a negative value. We conjecture that in this case, the energy dissipation caused by H-bond breaking becomes the primary resistance to the boundary slip, resulting in a slip length that approaches or equals zero. This type of slip behavior is similar to the no-slip boundary condition or the defect slip boundary condition (Martini et al. 2008), where the definition of the characteristic length d_{HB} may not be

applicable. As the pressure gradient gradually increases, the negative impact of H-bonds on the slip length diminishes, and the slip length increases. Then, the average slip velocity and slip length of the interfacial water layer can be defined and calculated using Eq. (15).

To illustrate the evolution of slip length with variations in the surface functional group concentrations, we calculated the two-dimensional distribution of interfacial slip velocity at the same driving force but different concentrations of hydroxyl functional groups c_{OH} on the graphene surface, as shown in Fig. 8. The slip velocity is significantly decreased for the water flows in the vicinity of hydroxyl groups. A clear contrast in the boundary velocity is evident when comparing the channel walls with no functional groups and extremely low functional group concentration ($c_{\text{OH}} = 0$ and 0.4%). Even a tiny number of hydroxyl groups exert a noticeable resistance, reducing the quite small slip velocity of the interfacial water layer. As the c_{OH} increases to 5%, the resistance affected by the hydroxyl groups spans the entire wall surface region, resulting in significant decreasing of the slip velocity.

The differences in the water velocity profiles along the y-direction at different functional group concentrations. Figure 9a presents the velocity distribution within channels with different functional group concentrations at a driving force of $f = 0.05$ kcal/(mol Å). It can be observed that both slip length and slip velocity decrease as the hydroxyl group concentration increases. The inset of Fig. 9 depicts the relationship between the slip velocity and the functional group concentration. It can be seen that even adding a very low concentration of functional groups ($c_{\text{OH}} = 0.4\%$) on the graphene wall can reduce the slip velocity by 32.5%. This obstructive effect of functional groups has also been observed in previous studies (Nair et al. 2012; Wei et al. 2014a). Furthermore, for different magnitudes of driving force, the obstruction on the boundary slip by a tiny number of hydroxyl groups remains significant. Figure 9b compares the case with a functional group concentration of $c_{\text{OH}} = 0.4\%$ to the case without any functional groups at different magnitudes of driving force. For example, at a driving force of $f = 0.01$ kcal/(mol Å), the slip velocity within a smooth channel is approximately 2 m/s, but the presence of a tiny number of hydroxyl groups ($c_{\text{OH}} = 0.4\%$) reduces the slip velocity to nearly zero.

Some studies in the literature suggest that the interaction of surface functional groups with fluids includes both van der Waals forces and H-bonding forces (Eslami et al. 2013; Eslami and Heydari 2014). When studying the H-bonding interaction separately, it is necessary to decouple these two effects. The H-bond is a primarily electrostatic force of attraction between a hydrogen atom and an electronegative oxygen atom bearing a lone pair of electrons. So we conducted new simulations, removing the charges of the

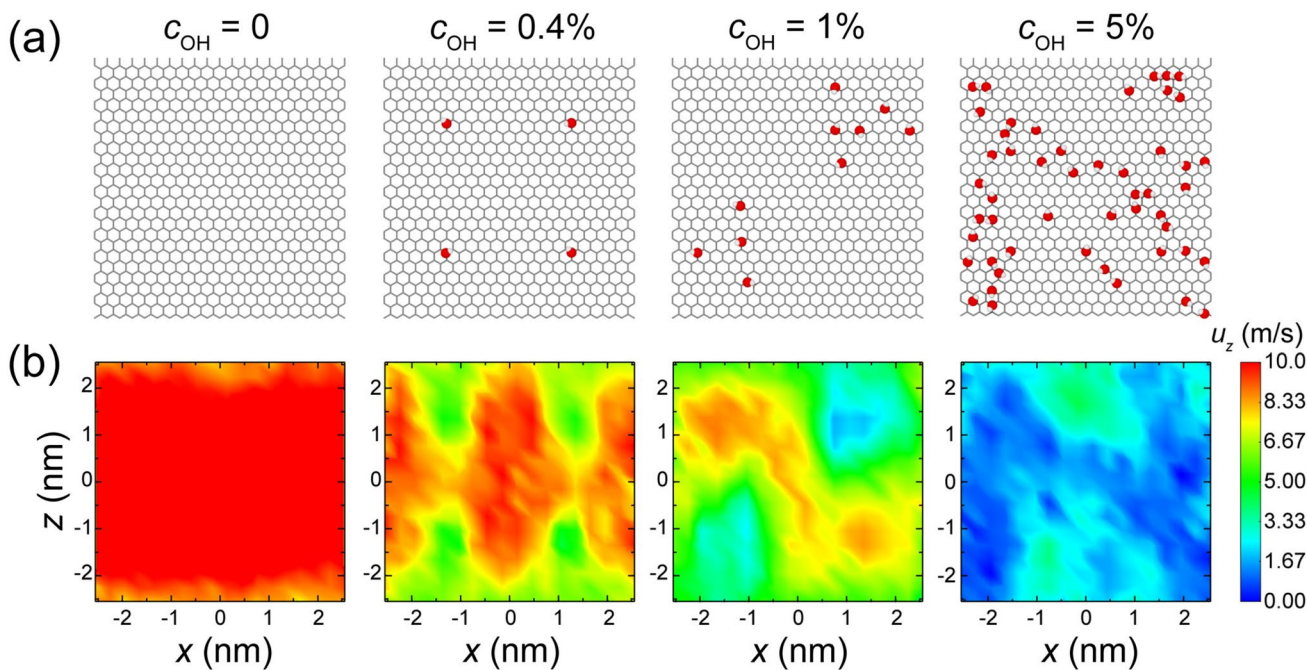


Fig. 8 **a** The graphene sheets with functional group concentration $c_{OH}=0-5\%$ and the corresponding flow boundary slip velocity distribution. **a** Top views of functional groups distributed on the graphene

sheets. **b** The distribution of water boundary slip velocity u_z in the xy -plane under driving force $f=0.05$ kcal/(mol Å)

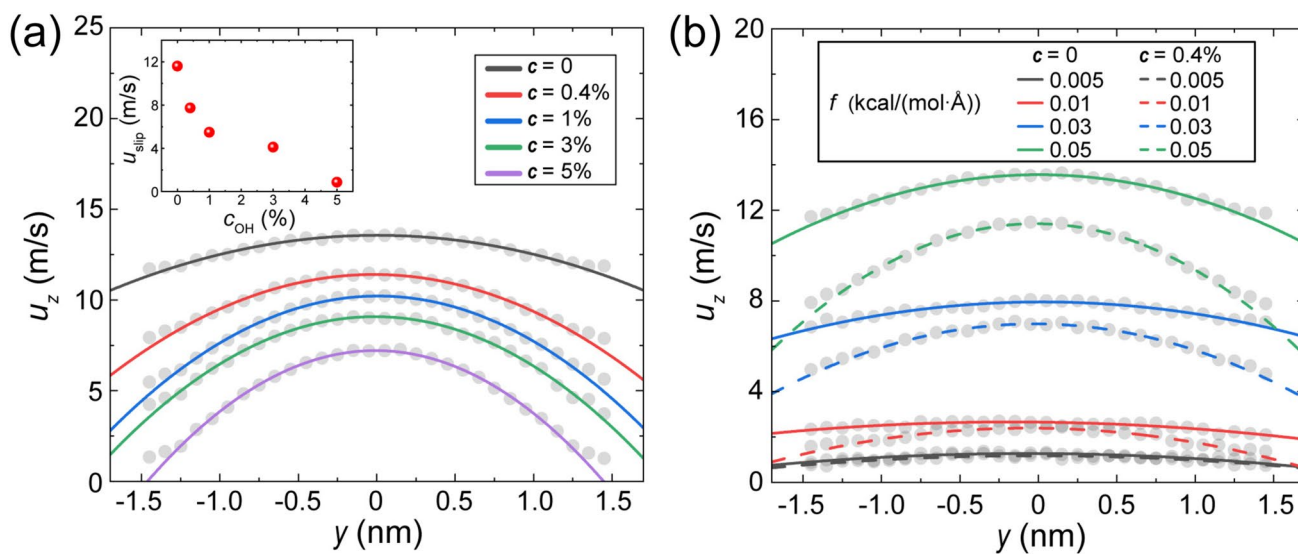


Fig. 9 **a** The profiles of water velocity u_z at different concentrations of hydroxyl groups under driving force $f=0.05$ kcal/(mol Å). The insert shows the boundary slip velocity u_{slip} versus the hydroxyl concentration c_{OH} . **b** The profiles of water velocity u_z in the channel of the functionalized walls (dashed line $c_{OH}=0.4\%$) and the pristine walls (solid line) under different driving forces

tration c_{OH} . **b** The profiles of water velocity u_z in the channel of the functionalized walls (dashed line $c_{OH}=0.4\%$) and the pristine walls (solid line) under different driving forces

functional groups on the channel walls and only considering the influence of van der Waals forces, effectively eliminating the effects of electrostatic forces and H-bonds. Then we calculated the slip velocity of water molecules near the wall and the distribution of density on the xy -plane under a

driving force of $f=0.03$ kcal/(mol Å). The results are shown in Fig. 10. Comparing these results with the previous ones, it is evident that after removing the influence of H-bonds, the slip velocities across the entire plane significantly increased. This increase is particularly noticeable near the functional

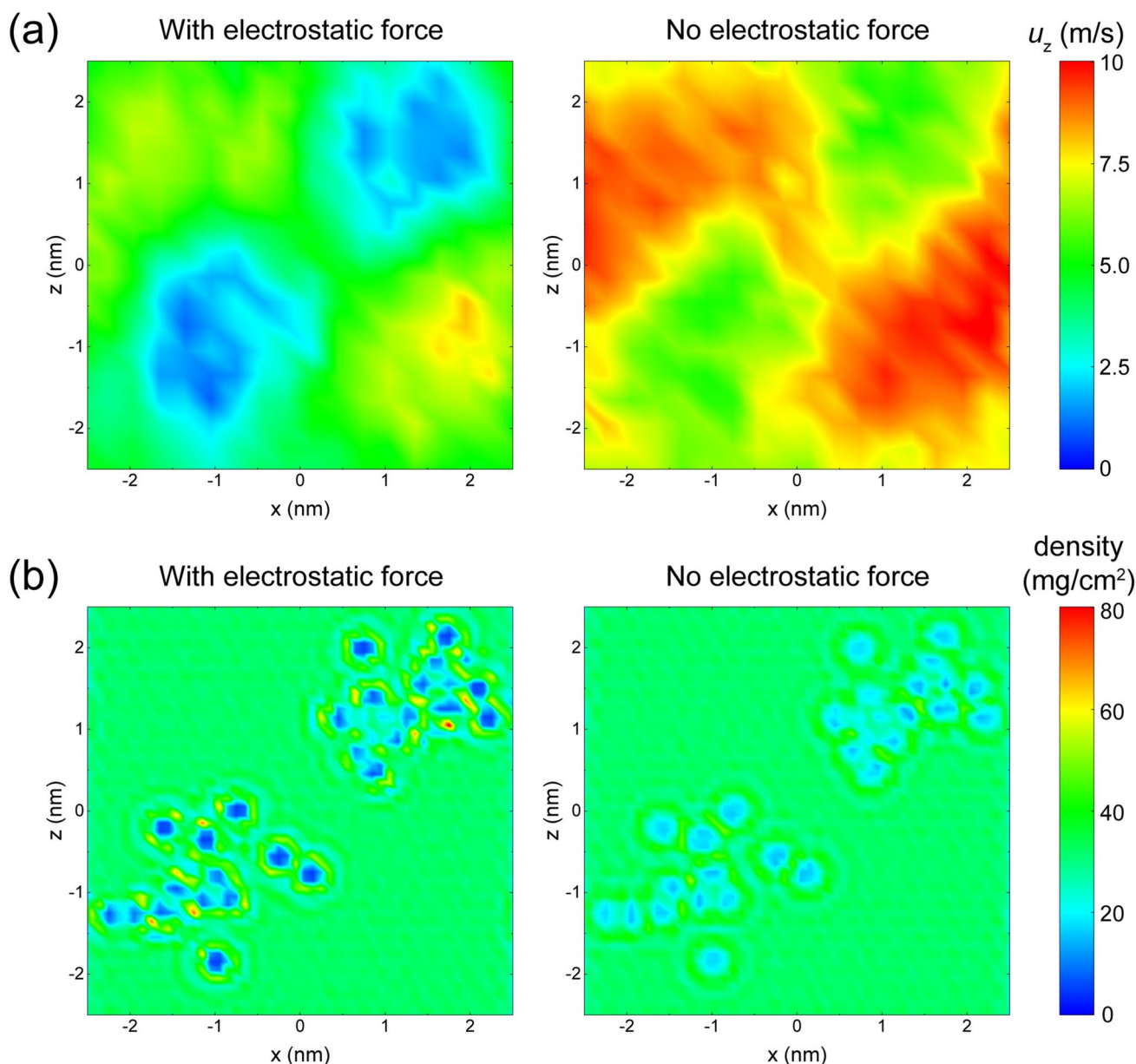


Fig. 10 **a** Z-direction boundary slip velocity and **b** density distribution of water in the xz -plane are shown. Water flows between the channel sheets with a functional group concentration of $c = 3\%$ and under driving forces $f = 0.05 \text{ kcal}/(\text{mol } \text{Å})$

groups, where the slip velocity rose from ~ 1.5 to $\sim 5.1 \text{ m/s}$. In addition, the water molecule density above the functional groups also increased, indicating a reduced hindrance effect of the functional groups on water flow.

Furthermore, we also investigated the relationship between the van der Waals and electrostatic forces, as well as the total force, with respect to the oxygen–oxygen atom distance d between individual water molecules and single functional groups. Figure 11 illustrates the variation of van der Waals forces, electrostatic forces, and the resultant total force as a function of d . It can be observed that within the range of $d = 2.6\text{--}7 \text{ Å}$, electrostatic forces

consistently make a significant contribution to the total force. Particularly, when water molecules and functional groups form relatively stable H-bonds, roughly in the range of $\sim 2.8 \text{ Å} \leq d \leq \sim 3.5 \text{ Å}$, electrostatic forces dominate the total force and serve as a crucial factor in H-bond formation.

All these findings underscore the significance of electrostatic forces within the functional groups and their interaction in forming H-bonds, emphasizing their profound impact on the motion of water molecules. This also highlights the pivotal role of H-bond interactions in boundary slip. While van der Waals forces have always been crucial in

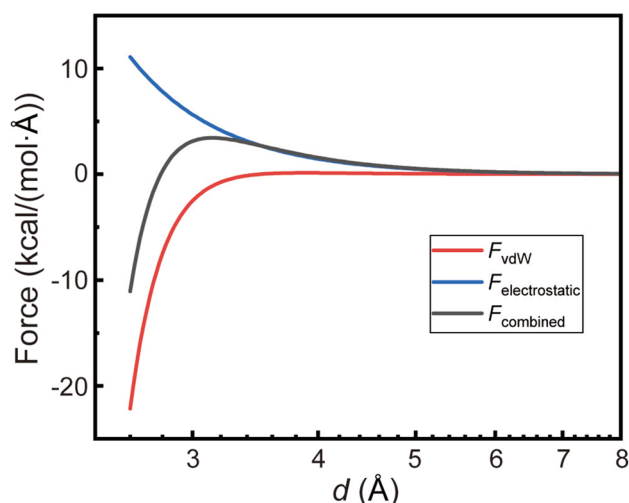


Fig. 11 The different types of forces between a water molecule and a hydroxyl group on the graphene sheet, in relation to the distance d between oxygen atoms

intermolecular interactions, especially in cases of extremely close molecular distances, the influence of H-bond forces induced by functional groups on boundary slip should not be underestimated.

4 Conclusion

In summary, we investigated the influence of hydroxyl-functionalized graphene nanochannel surfaces on the boundary slip, particularly concerning the dynamics of H-bonds formed between the hydroxyl groups and water molecules. We calculated the velocity of water molecules within the interfacial layer. The results show that functional groups significantly hinder the slip motion of nearby water molecules. At low driving forces, the water layer near the pristine region exhibits significant slip while the water layer near the functionalized region is difficult to slip. Furthermore, we analyzed the entire process of the boundary slip from an energetic perspective. At the interface, water molecules form H-bonds with functional groups on the wall surface. These H-bonds continuously form and break during the flow, resulting in energy dissipation. At the start of the slip, the energy required for water molecules to break the interfacial H-bonds is the primary dissipation mechanism. The frequency of H-bond breaking increases with the applied driving force. Finally, we propose a theoretical model for slip velocity based on energy balance that considers the influence of H-bond dynamics. At low driving forces, the slip is primarily influenced by H-bonds. As the driving force increases, the calculated slip length gradually transitions to the Navier slip length. Our research findings highlight that

the presence of low concentrations of functional groups has a greater impact on the flow behavior than expected.

Acknowledgements This work was financially supported by the National Natural Science Foundation of China (12241203, U22B2075) and the Youth Innovation Promotion Association CAS (2020449). The numerical calculations were performed on the supercomputing system in Hefei Advanced Computing Center and the Supercomputing Center of University of Science and Technology of China.

Author contributions JCL prepared Figs. 1, 2, 3, 5, 6, 7, 8, 9, 10, and 11. KLZ prepared Fig. 4. JCL and FCW wrote the main manuscript text and all authors reviewed the manuscript.

Data availability Data sets generated during the current study are available from the corresponding author on reasonable request.

Declarations

Conflict of interest The authors declare no conflict of interest.

References

- Abascal JLF, Vega C (2005) A general purpose model for the condensed phases of water: TIP4P/2005. *J Chem Phys* 123:234505. <https://doi.org/10.1063/1.2121687>
- Argyris D, Tummala NR, Striolo A, Cole DR (2008) Molecular structure and dynamics in thin water films at the silica and graphite surfaces. *J Phys Chem C* 112:13587–13599. <https://doi.org/10.1021/jp803234a>
- Berendsen HJC, Grigera JR, Straatsma TP (1987) The missing term in effective pair potentials. *J Phys Chem* 91:6269–6271. <https://doi.org/10.1021/j100308a038>
- Bocquet L, Barrat J-L (2007) Flow boundary conditions from nano- to micro-scales. *Soft Matter* 3:685–693. <https://doi.org/10.1039/B616490K>
- Bocquet L, Barrat J-L (2013) On the Green–Kubo relationship for the liquid–solid friction coefficient. *J Chem Phys* 139:044704. <https://doi.org/10.1063/1.4816006>
- Bocquet L, Charlaix E (2010) Nanofluidics, from bulk to interfaces. *Chem Soc Rev* 39:1073–1095. <https://doi.org/10.1039/B909366B>
- Chen B, Jiang H, Liu X, Hu X (2017) Observation and analysis of water transport through graphene oxide interlamination. *J Phys Chem C* 121:1321–1328. <https://doi.org/10.1021/acs.jpcc.6b09753>
- Eijkel JCT, van den Berg A (2005) Nanofluidics: What is it and what can we expect from it? *Microfluid Nanofluidics* 1:249–267. <https://doi.org/10.1007/s10404-004-0012-9>
- Erickson K, Erni R, Lee Z et al (2010) Determination of the local chemical structure of graphene oxide and reduced graphene oxide. *Adv Mater* 22:4467–4472. <https://doi.org/10.1002/adma.20100732>
- Eslami H, Heydari N (2014) Hydrogen bonding in water nanoconfined between graphene surfaces: a molecular dynamics simulation study. *J Nanoparticle Res* 16:1–10. <https://doi.org/10.1007/s11051-013-2154-8>
- Eslami H, Müller-Plathe F (2010) Viscosity of nanoconfined polyamide-6,6 oligomers: atomistic reverse nonequilibrium molecular dynamics simulation. *J Phys Chem B* 114:387–395. <https://doi.org/10.1021/jp908659w>
- Eslami H, Rahimi M, Müller-Plathe F (2013) Molecular dynamics simulation of a silica nanoparticle in oligomeric poly(methyl methacrylate): a model system for studying the interphase thickness

- in a polymer–nanocomposite via different properties. *Macromolecules* 46:8680–8692. <https://doi.org/10.1021/ma401443v>
- Falk K, Sedlmeier F, Joly L et al (2010) Molecular origin of fast water transport in carbon nanotube membranes: Superlubricity versus curvature dependent friction. *Nano Lett* 10:4067–4073. <https://doi.org/10.1021/nl1021046>
- Fang C, Wu X, Yang F, Qiao R (2018) Flow of quasi-two dimensional water in graphene channels. *J Chem Phys* 148:064702. <https://doi.org/10.1063/1.5017491>
- Figoli A, Hoinkis J, Altinkaya SA, Bundschuh J (2017) Application of nanotechnology in membranes for water treatment. CRC Press, London
- González MA, Abascal JLF (2010) The shear viscosity of rigid water models. *J Chem Phys* 132:096101. <https://doi.org/10.1063/1.3330544>
- Grosjean B, Pean C, Siria A et al (2016) Chemisorption of hydroxide on 2D materials from DFT calculations: graphene versus hexagonal boron nitride. *J Phys Chem Lett* 7:4695–4700. <https://doi.org/10.1021/acs.jpcclett.6b02248>
- Guo S, Meshot ER, Kuykendall T et al (2015) Nanofluidic transport through isolated carbon nanotube channels: advances, controversies, and challenges. *Adv Mater* 27:5726–5737. <https://doi.org/10.1002/adma.201500372>
- Guo S, Garaj S, Bianco A, Ménard-Moyon C (2022) Controlling covalent chemistry on graphene oxide. *Nat Rev Phys* 4:247–262. <https://doi.org/10.1038/s42254-022-00422-w>
- Ho TA, Striolo A (2014) Molecular dynamics simulation of the graphene–water interface: comparing water models. *Mol Simul* 40:1190–1200. <https://doi.org/10.1080/08927022.2013.854893>
- Hummer G, Rasaiah JC, Noworyta JP (2001) Water conduction through the hydrophobic channel of a carbon nanotube. *Nature* 414:188–190. <https://doi.org/10.1038/35102535>
- Irving JH, Kirkwood JG (2004) The statistical mechanical theory of transport processes. IV. The equations of hydrodynamics. *J Chem Phys* 18:817–829. <https://doi.org/10.1063/1.1747782>
- Joly L, Tocci G, Merabia S, Michaelides A (2016) Strong coupling between nanofluidic transport and interfacial chemistry: how defect reactivity controls liquid–solid friction through hydrogen bonding. *J Phys Chem Lett* 7:1381–1386. <https://doi.org/10.1021/acs.jpcclett.6b00280>
- Jorgensen WL, Maxwell DS, Tirado-Rives J (1996) Development and testing of the OPLS all-atom force field on conformational energetics and properties of organic liquids. *J Am Chem Soc* 118:11225–11236. <https://doi.org/10.1021/ja9621760>
- Kalluri RK, Ho TA, Biener J et al (2013) Partition and structure of aqueous NaCl and CaCl₂ electrolytes in carbon-slit electrodes. *J Phys Chem C* 117:13609–13619. <https://doi.org/10.1021/jp4002127>
- Kannam SK, Todd BD, Hansen JS, Daivis PJ (2013) How fast does water flow in carbon nanotubes? *J Chem Phys* 138:094701. <https://doi.org/10.1063/1.4793396>
- Kavokine N, Netz RR, Bocquet L (2021) Fluids at the nanoscale: from continuum to subcontinuum transport. *Annu Rev Fluid Mech* 53:377–410. <https://doi.org/10.1146/annurev-fluid-071320-095958>
- Li J, Zhu Y, Xia J et al (2021) Anomalously low friction of confined monolayer water with a quadrilateral structure. *J Chem Phys* 154:224508. <https://doi.org/10.1063/5.0053361>
- Luzar A, Chandler D (1996a) Effect of environment on hydrogen bond dynamics in liquid water. *Phys Rev Lett* 76:928–931. <https://doi.org/10.1103/PhysRevLett.76.928>
- Luzar A, Chandler D (1996b) Hydrogen-bond kinetics in liquid water. *Nature* 379:55–57. <https://doi.org/10.1038/379055a0>
- Majumder M, Chopra N, Hinds BJ (2011) Mass transport through carbon nanotube membranes in three different regimes: ionic diffusion and gas and liquid flow. *ACS Nano* 5:3867–3877. <https://doi.org/10.1021/nn200222g>
- Mark P, Nilsson L (2001) Structure and dynamics of the TIP3P, SPC, and SPC/E water models at 298 K. *J Phys Chem A* 105:9954–9960. <https://doi.org/10.1021/jp003020w>
- Martini A, Roxin A, Snurr RQ et al (2008) Molecular mechanisms of liquid slip. *J Fluid Mech* 600:257–269. <https://doi.org/10.1017/S0022112008000475>
- Michaelides A (2016) Slippery when narrow. *Nature* 537:171–172. <https://doi.org/10.1038/537171a>
- Mouhat F, Coudert F-X, Bocquet M-L (2020) Structure and chemistry of graphene oxide in liquid water from first principles. *Nat Commun* 11:1566. <https://doi.org/10.1038/s41467-020-15381-y>
- Nair RR, Wu HA, Jayaram PN et al (2012) Unimpeded permeation of water through helium-leak-tight graphene-based membranes. *Science* 335:442–444. <https://doi.org/10.1126/science.1211694>
- Navier C (1823) Mémoire sur les lois du mouvement des fluides. *Mém L'académie R Sci L'institut Fr* 6:389–440
- Plimpton S (1995) Fast parallel algorithms for short-range molecular dynamics. *J Comput Phys* 117:1–19. <https://doi.org/10.1006/jcph.1995.1039>
- Sala J, Guàrdia E, Martí J (2012) Specific ion effects in aqueous electrolyte solutions confined within graphene sheets at the nanometric scale. *Phys Chem Chem Phys* 14:10799–10808. <https://doi.org/10.1039/C2CP40537G>
- Schoch RB, Han J, Renaud P (2008) Transport phenomena in nanofluidics. *Rev Mod Phys* 80:839–883. <https://doi.org/10.1103/RevModPhys.80.839>
- Secchi E, Marbach S, Niguès A et al (2016) Massive radius-dependent flow slippage in carbon nanotubes. *Nature* 537:210–213. <https://doi.org/10.1038/nature19315>
- Smith PE, van Gunsteren WF (1993) The viscosity of SPC and SPC/E water at 277 and 300 K. *Chem Phys Lett* 215:315–318. [https://doi.org/10.1016/0009-2614\(93\)85720-9](https://doi.org/10.1016/0009-2614(93)85720-9)
- Taherian F, Marcon V, van der Vegt NFA, Leroy F (2013) What is the contact angle of water on graphene? *Langmuir* 29:1457–1465. <https://doi.org/10.1021/la304645w>
- Tocci G, Joly L, Michaelides A (2014) Friction of water on graphene and hexagonal boron nitride from ab initio methods: very different slippage despite very similar interface structures. *Nano Lett* 14:6872–6877. <https://doi.org/10.1021/nl502837d>
- Vijayaraghavan V, Wong CH (2014) Transport characteristics of water molecules in carbon nanotubes investigated by using molecular dynamics simulation. *Comput Mater Sci* 89:36–44. <https://doi.org/10.1016/j.commatsci.2014.03.025>
- Wei N, Peng X, Xu Z (2014a) Breakdown of fast water transport in graphene oxides. *Phys Rev E* 89:012113. <https://doi.org/10.1103/PhysRevE.89.012113>
- Wei N, Peng X, Xu Z (2014b) Understanding water permeation in graphene oxide membranes. *ACS Appl Mater Interfaces* 6:5877–5883. <https://doi.org/10.1021/am500777b>
- Whitby M, Quirke N (2007) Fluid flow in carbon nanotubes and nanopipes. *Nat Nanotechnol* 2:87–94. <https://doi.org/10.1038/nnano.2006.175>
- Wu Y, Aluru NR (2013) Graphitic carbon–water nonbonded interaction parameters. *J Phys Chem B* 117:8802–8813. <https://doi.org/10.1021/jp402051t>
- Wu Y, Tepper HL, Voth GA (2006) Flexible simple point-charge water model with improved liquid-state properties. *J Chem Phys* 124:024503. <https://doi.org/10.1063/1.2136877>
- Yan J-A, Chou MY (2010) Oxidation functional groups on graphene: Structural and electronic properties. *Phys Rev B* 82:125403. <https://doi.org/10.1103/PhysRevB.82.125403>
- Yang JZ, Wu X, Li X (2012) A generalized Irving–Kirkwood formula for the calculation of stress in molecular dynamics models. *J Chem Phys* 137:134104. <https://doi.org/10.1063/1.4755946>

- Ye H, Zhang H, Zheng Y, Zhang Z (2011) Nanoconfinement induced anomalous water diffusion inside carbon nanotubes. *Microfluid Nanofluidics* 10:1359–1364. <https://doi.org/10.1007/s10404-011-0772-y>
- Ye H, Wang J, Zheng Y et al (2021) Machine learning for reparameterization of four-site water models: TIP4P-BG and TIP4P-BGT. *Phys Chem Chem Phys* 23:10164–10173. <https://doi.org/10.1039/D0CP05831A>
- Zhang Z, Li S, Mi B et al (2020) Surface slip on rotating graphene membrane enables the temporal selectivity that breaks the permeability-selectivity trade-off. *Sci Adv* 6:eaba9471. <https://doi.org/10.1126/sciadv.aba9471>

Zhao YP (2012) *Physical mechanics of surfaces and interfaces*. Science Press, Beijing

Publisher's Note Springer Nature remains neutral with regard to jurisdictional claims in published maps and institutional affiliations.

Springer Nature or its licensor (e.g. a society or other partner) holds exclusive rights to this article under a publishing agreement with the author(s) or other rightsholder(s); author self-archiving of the accepted manuscript version of this article is solely governed by the terms of such publishing agreement and applicable law.